

Article

Facile Preparation and Promising Hydrothermal Stability of Spherical γ -Alumina Support with High Specific Surface Area

Yi Zhang, Yimin Lv, Yufan Mo, Huiyu Li, Pinggui Tang, Dianqing Li * and Yongjun Feng * 

State Key Laboratory of Chemical Resource Engineering, Beijing Engineering Center for Hierarchical Catalysts, Beijing University of Chemical Technology, Beijing 100029, China

* Correspondence: lidq@mail.buct.edu.cn (D.L.); yjfeng@mail.buct.edu.cn (Y.F.)

Abstract: It is of great importance to develop a spherical γ -alumina support with high hydrothermal stability to be used in platinum reforming catalyst processes. The porous pseudo-boehmite powder with a high surface area was first synthesized via a simple separate nucleation and aging steps method, and was then used as a precursor to produce a spherical γ -Al₂O₃ support via an oil–ammonia column method. The as-synthesized pseudo-boehmite has a substantially greater specific surface area of 336.0 m²·g^{−1} in comparison with the commercial Sasol boehmite powder (293.0 m²·g^{−1}) from Sasol Chemicals. In addition, the as-prepared spherical γ -Al₂O₃ support derived from the as-synthesized pseudo-boehmite also possesses a higher specific surface area of 280.0 m²·g^{−1} compared to the corresponding Sasol sample. Moreover, the as-prepared spherical γ -Al₂O₃ balls demonstrate a much higher specific surface area of 185.0 m²·g^{−1} compared with the Sasol sample of 142.0 m²·g^{−1} after hydrothermal tests at 600 °C, suggesting its promising application in the chemical industry.

Keywords: pseudo-boehmite; spherical γ -alumina; hydrothermal stability; high specific surface area; separate nucleation and aging steps method; oil–ammonia column method



Citation: Zhang, Y.; Lv, Y.; Mo, Y.; Li, H.; Tang, P.; Li, D.; Feng, Y. Facile Preparation and Promising Hydrothermal Stability of Spherical γ -Alumina Support with High Specific Surface Area. *Catalysts* **2022**, *12*, 1416. <https://doi.org/10.3390/catal12111416>

Academic Editor: Leonarda Liotta

Received: 23 October 2022

Accepted: 8 November 2022

Published: 11 November 2022

Publisher's Note: MDPI stays neutral with regard to jurisdictional claims in published maps and institutional affiliations.



Copyright: © 2022 by the authors. Licensee MDPI, Basel, Switzerland. This article is an open access article distributed under the terms and conditions of the Creative Commons Attribution (CC BY) license (<https://creativecommons.org/licenses/by/4.0/>).

1. Introduction

Petroleum-based fossil fuels are still the most widely used energy source, and heterogeneous catalysts are indispensable in the petrochemical industry, particularly in the platinum reforming catalyst process [1,2]. Because of its high specific surface area and distinctive pore structure, γ -Al₂O₃ is by far the most commonly utilized inorganic material as a catalyst or catalytic support for heterogeneous catalysis [3–6]. Spherical γ -Al₂O₃ balls have attracted significant attention due to their uniform morphology, large specific surface area, small bulk density, and excellent fluidity [7,8].

Unfortunately, γ -Al₂O₃ can easily adsorb water molecules and can be transformed into hydrated alumina in water steam at high temperatures, giving rise to the reduction in the specific surface area and destruction of the pore structure [9]. Many methods, such as element doping [10–12], and optimization of the synthesis process [13–16], have been adopted to improve the hydrothermal stability of γ -Al₂O₃. For example, López Pérez et al. [17] developed a condensation-enhanced self-assembly and pyrolysis crystallization method to produce transition alumina with enhanced hydrothermal stability. Moreover, Fujisaki et al. [18] employed a sol-gel method to prepare La₂O₃- and/or Ga₂O₃-doped γ -Al₂O₃, and revealed that La₂O₃ on the grain surface of Ga₂O₃-Al₂O₃ solid solution improved the hydrothermal stability of γ -Al₂O₃. Additionally, Gu et al. [19] adopted a chemical vapor deposition method to fabricate silica-doped alumina with high hydrothermal stability at 873 K. However, most of the reported methods involve complicated preparation processes or some impurities, which may cause a negative effect on the catalytic performance. Therefore, it is desirable to develop a simple method to prepare spherical γ -Al₂O₃ balls with high hydrothermal stability.

Herein, a simple process composed of the preparation of pseudo-boehmite (PB) with a high specific surface area and subsequent modeling of pseudo-boehmite into spherical

γ -Al₂O₃ balls was proposed. At first, pseudo-boehmite powder with a specific surface area of 336.0 m²·g⁻¹ was synthesized via a simple separate nucleation and aging steps method developed in our laboratory [20–22], which can be used to prepare nanomaterials on a large scale, e.g., 3500 t/a layered double hydroxides. In this method, all the nuclei were formed in a few seconds, and then the nuclei were crystallized and grown at the same time. Subsequently, pseudo-boehmite sol was prepared and dropped into an oil-ammonia column to form pseudo-boehmite gel balls, which were then dried and calcined at 600 °C to produce spherical γ -Al₂O₃ balls. Promisingly, the obtained spherical γ -Al₂O₃ balls possess the advantages of a high specific surface area, and excellent hydrothermal stability, indicating their hopeful application in the platinum reforming catalyst process.

2. Results and Discussion

2.1. Morphologies and Structure of PB Powder

Figure 1 shows SEM and TEM images of PB and Sasol boehmite (SB) samples. PB powder (Figure 1a,c) consists of loosely stacked nanoparticles and an abundant pore structure, and some small particles assemble into nanofibers. In contrast, SB powder is composed of tightly integrated nanoparticles with less pores (Figure 1b,d).

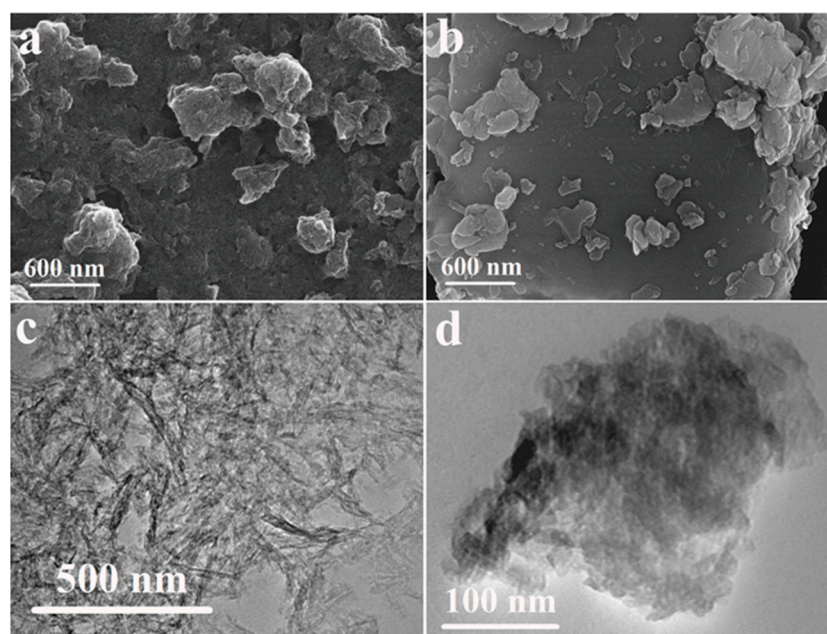


Figure 1. SEM and TEM images of PB (a,c) and SB (b,d) samples.

Powder X-ray diffraction (XRD) pattern measurements were performed to investigate the crystal structure of PB and SB powder, and Figure 2a displays the powder XRD patterns of both samples. Here, there are six diffraction peaks that appear at 14.39, 28.13, 38.27, 48.93, 54.94 and 63.69°/2 θ in the XRD pattern of SB powder, which are consistent with the (020), (201), (130), (002), (151) and (200) diffraction peaks of pseudo-boehmite [23]. One can observe that the XRD patterns of PB are similar to those of SB, suggesting that the as-synthesized PB has the same crystal structure as the SB powder. Fourier transform infrared spectroscopy (FT-IR) characterization was conducted to further investigate the composition of PB. As depicted in Figure 2b, the spectrum of PB is also similar to that of SB powder, indicating that PB and SB have the same characteristic functional groups. Specifically, the two broad bands at 3400 and 3093 cm⁻¹ can be assigned to the stretch vibration of the hydroxyl groups. The absorption band at 1078 cm⁻¹ is attributed to the symmetrical bending vibration of the Al-O-H group, and the two adsorption bands at 626 and 485 cm⁻¹ could be ascribed to the vibration of the Al-O bond.

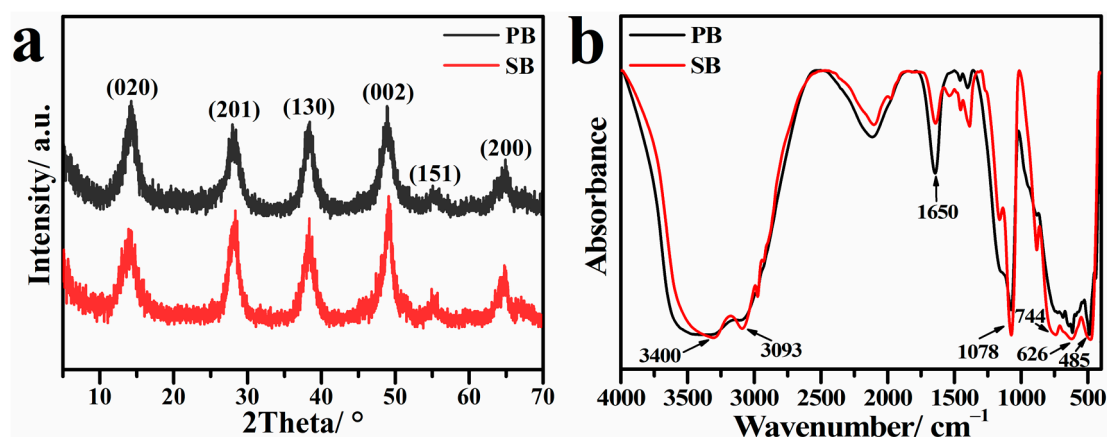


Figure 2. Powder XRD patterns (a) and FT-IR spectra (b) of PB and SB powder.

2.2. Pore Structure of PB Powder

The pore structure of PB and SB was evaluated by the low-temperature N_2 adsorption-desorption method. Figure 3a demonstrates that the PB sample has similar adsorption and desorption isotherms and a similar type H3 hysteresis loop to the SB sample, suggesting the presence of abundant mesopores in both PB and SB. The calculated Brunauer-Emmett Teller (BET) specific surface area is ca. $336.0 \text{ m}^2 \cdot \text{g}^{-1}$ for the as-synthesized PB, which is larger than that of SB powder ($293.0 \text{ m}^2 \cdot \text{g}^{-1}$). Figure 3b shows the pore size distribution curves of PB and SB obtained according to the Barret-Joyner-Halenda (BJH) method. In comparison, the as-prepared PB sample has narrower pore size distribution, ranging from 3 to 8 nm, in comparison to the SB sample's distribution from 2 to 10 nm, possibly resulting from its small and homogeneous particle size. The results suggest that the separate nucleation and aging steps method is useful to produce porous pseudo-boehmite with a large specific surface area and narrow pores.

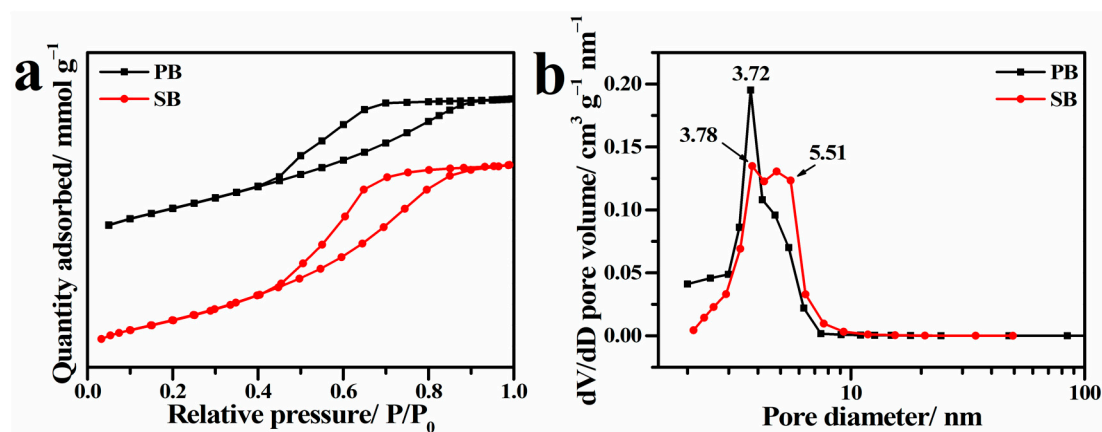


Figure 3. Low-temperature nitrogen adsorption isotherms (a) and corresponding pore size distribution curves (b) of PB and SB samples.

2.3. Morphologies and Structure of Spherical $\gamma\text{-Al}_2\text{O}_3$ Balls

Spherical $\gamma\text{-Al}_2\text{O}_3$ balls, marked as $\text{Al}_2\text{O}_3\text{-I}$, were modeled using an oil-ammonia column method with the PB powder as the precursor, and calcined at 600°C under air atmosphere for 4 h. Figure 4a,b show the photographs of $\text{Al}_2\text{O}_3\text{-I}$ from the as-prepared PB sample and commercial $\gamma\text{-Al}_2\text{O}_3\text{-S}$ balls from Sosal Chemicals, respectively. The $\text{Al}_2\text{O}_3\text{-I}$ balls possess uniform sizes with diameters of $2.0 \pm 0.1 \text{ mm}$, and smooth surfaces. SEM characterization was further carried out to investigate the microstructures of the obtained $\gamma\text{-Al}_2\text{O}_3$ balls. Figure 4c,d display the scanning electron microscope (SEM) images of $\text{Al}_2\text{O}_3\text{-S}$ with smooth outside surfaces and porous inside structures, which are different from those

of $\text{Al}_2\text{O}_3\text{-I}$, as shown in Figure 4e,f. One can observe that $\text{Al}_2\text{O}_3\text{-I}$ consists of many particles, and its porous structure may be a result of the space among neighboring particles.

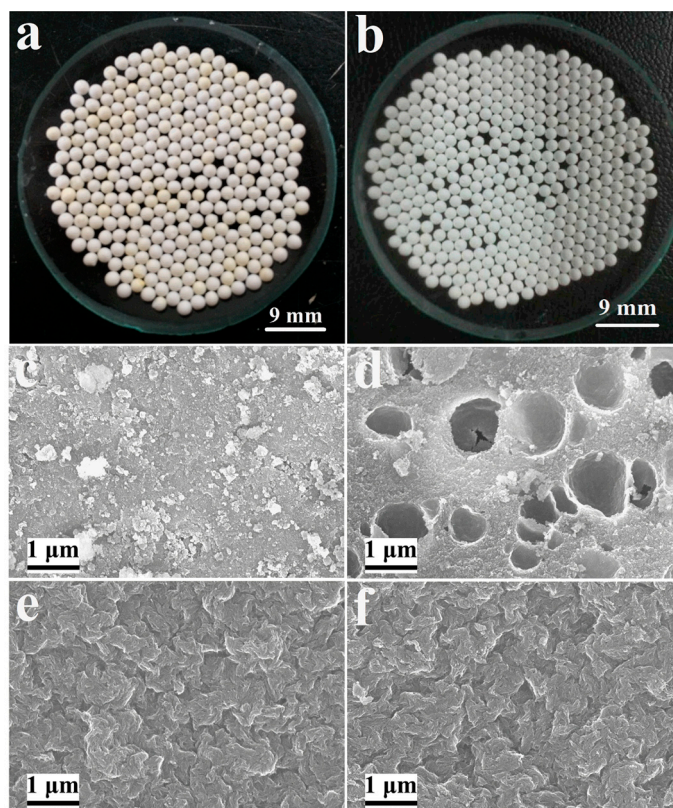


Figure 4. Photograph of $\text{Al}_2\text{O}_3\text{-I}$ (a) and $\text{Al}_2\text{O}_3\text{-S}$ (b); SEM image of $\text{Al}_2\text{O}_3\text{-S}$ (c,d) and $\text{Al}_2\text{O}_3\text{-I}$ (e,f).

Figure 5 depicts the XRD patterns of the powder ground from both of the $\text{Al}_2\text{O}_3\text{-I}$ and $\text{Al}_2\text{O}_3\text{-S}$ samples, respectively. Evidently, the diffraction peaks of PB and SB disappear, while a series of new diffraction peaks ascribed to $\gamma\text{-Al}_2\text{O}_3$ appear, and the corresponding hkl values are marked on the graph, suggesting the successful transformation from pseudo-boehmite precursors into $\gamma\text{-Al}_2\text{O}_3$ after calcination at $600\text{ }^\circ\text{C}$.

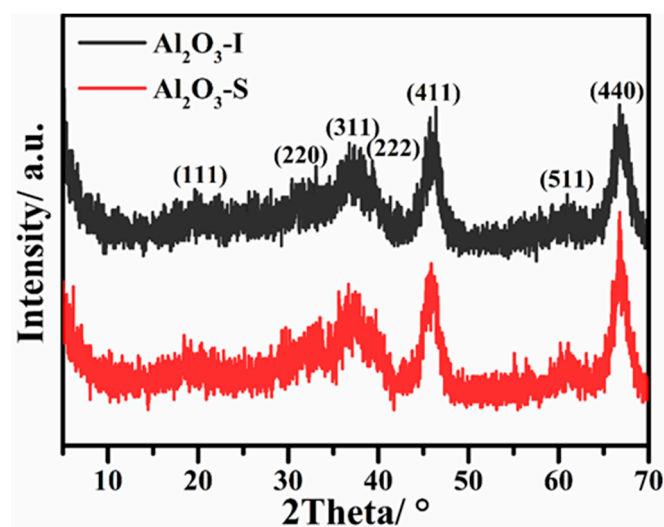


Figure 5. Powder XRD patterns of $\text{Al}_2\text{O}_3\text{-I}$ and $\text{Al}_2\text{O}_3\text{-S}$ ground powder.

2.4. Hydrothermal Stability of γ - Al_2O_3

The hydrothermal stability of γ - Al_2O_3 as a catalyst support is crucial for its application in the platinum reforming catalyst process [24,25]. During this catalytic process, the catalysts have worse catalytic activity and selectivity when the surface area is below $140 \text{ m}^2 \cdot \text{g}^{-1}$. Figure 6 shows the low-temperature nitrogen adsorption–desorption isotherms (a, b), and the corresponding pore size distribution curves (c, d) for spherical Al_2O_3 -I (a, c) and Al_2O_3 -S (b, d) before and after hydrothermal treatment at 600°C , under water vapor. One can observe that the adsorption isotherms of Al_2O_3 -I and Al_2O_3 -S after hydrothermal treatment are similar to those of Al_2O_3 -I and Al_2O_3 -S before hydrothermal treatment. However, the desorption isotherms are somewhat different. The beginning desorption relative pressures of the samples after hydrothermal tests are slightly higher than the corresponding initial samples, which implies that the pore size becomes larger after hydrothermal treatment. The pore size distribution curves in Figure 6c,d further confirm this result. The pore size of Al_2O_3 -I increases from 7.2 nm to 10.8 nm after hydrothermal treatment for 48 h. Meanwhile, the pore size of Al_2O_3 -S increases from 7.2 nm to 8.7 nm. Moreover, the pore size distribution curves of both compounds show minimal changes after the first cycle, indicating that the pore structures remain stable after 48 h of hydrothermal treatment.

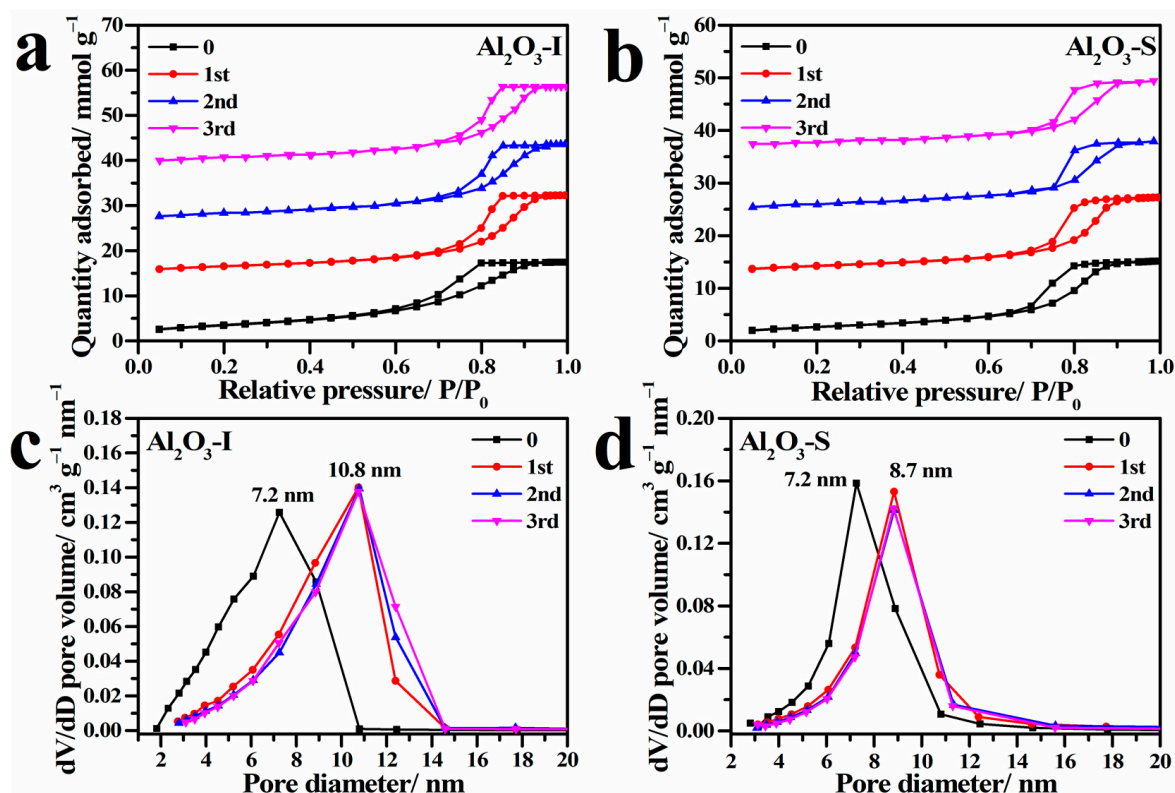


Figure 6. Adsorption–desorption isotherms and pore size distribution curves of Al_2O_3 -I (a,c) and Al_2O_3 -S (b,d) after hydrothermal treatment under water vapor at 600°C for 48 h (one cycle). Here, the 0, 1st, 2nd, and 3rd samples correspond to the samples that were calcined at 600°C for 4 h after the 0 to 3rd hydrothermal treatment cycles, respectively.

In addition, Figure 7 further demonstrates the BET specific surface areas of Al_2O_3 -I and Al_2O_3 -S after hydrothermal treatment. After hydrothermal treatment (one cycle is 48 h), the treated Al_2O_3 balls were calcined at 600°C for 4 h again for repeated hydrothermal treatment. The specific surface areas of Al_2O_3 -I and Al_2O_3 -S decrease from $280.0 \text{ m}^2 \cdot \text{g}^{-1}$ to $206.0 \text{ m}^2 \cdot \text{g}^{-1}$ and from $209.5 \text{ m}^2 \cdot \text{g}^{-1}$ to $180.0 \text{ m}^2 \cdot \text{g}^{-1}$, respectively, after the first cycle. One can observe that the specific surface areas of Al_2O_3 -I and Al_2O_3 -S decrease much more slowly in the second cycle in comparison with the first one, and then become more stable. Finally, the specific surface area of Al_2O_3 -I remained at $185.0 \text{ m}^2 \cdot \text{g}^{-1}$ after 4 cycles for 192 h,

which is much higher than that of $\text{Al}_2\text{O}_3\text{-S}$ for $142.0 \text{ m}^2 \cdot \text{g}^{-1}$, indicating that $\text{Al}_2\text{O}_3\text{-I}$ derived from the pseudo-boehmite prepared by the separate nucleation and aging steps method can retain a much larger specific surface area in comparison with the commercial powder from Sasol Chemicals. The larger specific surface area improves the catalytic performance of catalysts based on $\gamma\text{-Al}_2\text{O}_3$ supports, suggesting the promising application of $\text{Al}_2\text{O}_3\text{-I}$ in the chemical industry.

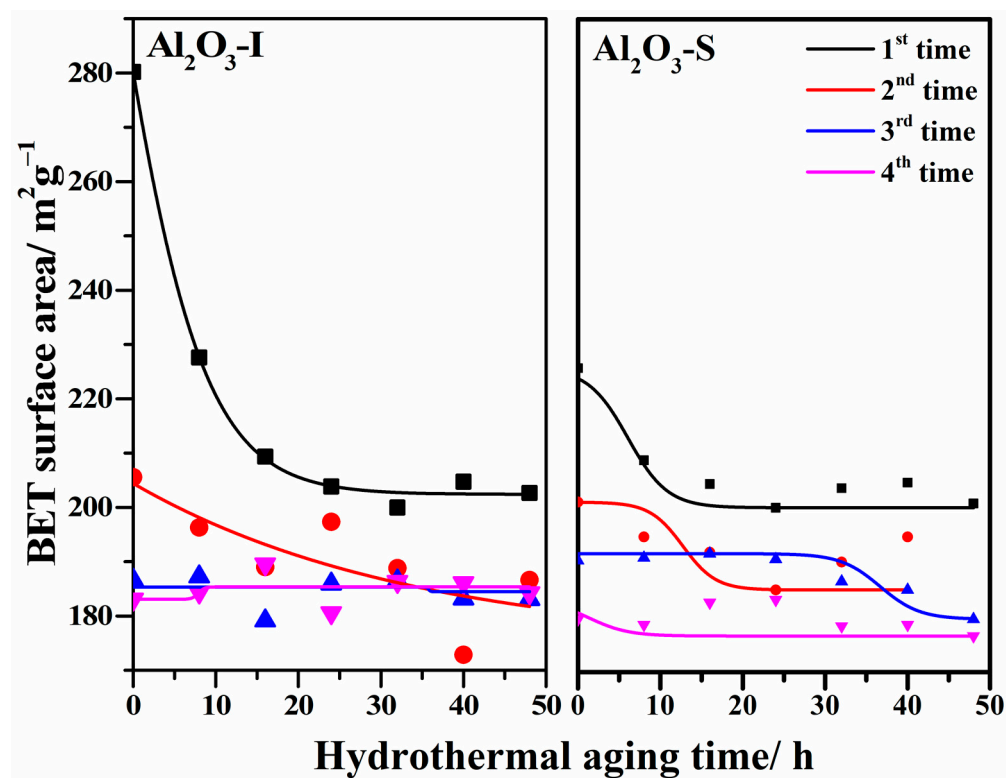


Figure 7. BET specific surface area variation in $\text{Al}_2\text{O}_3\text{-I}$ and $\text{Al}_2\text{O}_3\text{-S}$ after one to four cases of hydrothermal treatment under water vapor at 600°C for 48 h (one cycle).

3. Materials and Methods

3.1. Chemicals

Analytical grade aluminum sulfate ($\text{Al}_2(\text{SO}_4)_3 \cdot 18\text{H}_2\text{O}$), sodium metaaluminate (NaAlO_2), ammonia, nitric acid and alcohol were used without further purification. The commercial SB powder and $\text{Al}_2\text{O}_3\text{-S}$ balls were supplied by Sasol Chemicals.

3.2. Synthesis of Pseudo-Boehmite

Pseudo-boehmite (PB) was synthesized via a simple separate nucleation and aging steps method by using $\text{Al}_2(\text{SO}_4)_3 \cdot 18\text{H}_2\text{O}$ and NaAlO_2 as the reagents. First, 6.665 g (0.01 mol) of $\text{Al}_2(\text{SO}_4)_3 \cdot 18\text{H}_2\text{O}$ and 4.918 g (0.06 mol) of NaAlO_2 were dissolved in 100 mL of deionized water to form homogenous solutions, respectively. A heating mantle was used to heat $\text{Al}_2(\text{SO}_4)_3$ solution to 85°C , and then the $\text{Al}_2(\text{SO}_4)_3$ and NaAlO_2 solutions were pumped into a rotating liquid membrane reactor at the same rate. The obtained mixture was transferred into a three-necked flask and stirred for 6 h at 100°C . The PB precipitates were dried at 60°C for 24 h after washing and centrifugating repeatedly with deionized water and alcohol.

3.3. Preparation of Spherical $\gamma\text{-Al}_2\text{O}_3$ Balls

Spherical $\gamma\text{-Al}_2\text{O}_3$ balls were prepared via an oil–ammonia column modeling method. Specifically, 12.0 g of the as-synthesized PB was dispersed in 28.0 mL of deionized water by magnetic stirring for 0.5 h, and the suspension was heated to 100°C . After this, 21.0 g

of dilute nitric acid solution (3 wt%) was added dropwise into the suspension under vigorous stirring to achieve a $H^+ : Al^{3+}$ ratio of 0.05: 1. To obtain pseudo-boehmite sol, the resultant slurry was continuously stirred for 4 h at 100 °C. After cooling down to ambient temperature, the as-prepared sol was dropped into an oil–ammonia column by an injector, and the formed gel spheres were aged for 4 h to produce spherical pseudo-boehmite gel balls. The formed gel balls were washed with deionized water 8 times, followed by drying overnight at 90 °C. Finally, the as-prepared spherical pseudo-boehmite gel balls were calcined at 600 °C for 4 h to form spherical γ - Al_2O_3 balls, which were denoted as Al_2O_3 -I.

3.4. Hydrothermal Stability Evaluation

The hydrothermal stability of spherical γ - Al_2O_3 balls was tested at 600 °C under a continuous water vapor steam in a tube furnace, and a portion of the balls were taken out for characterization every 8 h. After testing for 48 h, the spherical γ - Al_2O_3 balls were removed and then calcined at 600 °C for 4 h. The testing and calcination cycle was repeated three times.

3.5. Characterizations

Powder X-ray diffraction (XRD) patterns of the samples were recorded using an Ni-filtered Cu - $K\alpha$ radiation (Rigaku D/max-Ultima III) X-ray diffractometer with a scan speed of $10^\circ \text{ min}^{-1}$. Morphologies of the samples were investigated by a scanning electron microscope (SEM, Zeiss Supra 55) and high-resolution transmission electron microscopy (TME, JEOL JEM-2010 with an accelerating voltage of 200 kV). Fourier transform infrared spectroscopy (FT-IR) spectra of the samples were recorded on a FT-IR spectrometer (VECTOR 22, 4000–400 cm^{-1}). Pore structures were analyzed using the low-temperature nitrogen adsorption–desorption method and a Micromeritics ASAP 2390 volumetric adsorption analyzer.

4. Conclusions

In summary, pseudo-boehmite powder with a high specific surface area was successfully synthesized using the separate nucleation and aging steps method and spherical γ - Al_2O_3 balls with a high specific surface area were then obtained by an oil–ammonia column modeling method, using the obtained pseudo-boehmite as the precursor. The as-synthesized pseudo-boehmite has a high BET specific surface area of $336.0 \text{ m}^2 \cdot \text{g}^{-1}$ and a pore size of 3.72 nm, giving rise to the high specific surface area of γ - Al_2O_3 ($280.0 \text{ m}^2 \cdot \text{g}^{-1}$). Meanwhile, the prepared γ - Al_2O_3 balls retain a specific surface area of $185.0 \text{ m}^2 \cdot \text{g}^{-1}$ after four hydrothermal treatment cycles (192 h), which is much larger than that of the commercial powder from Sasol Chemicals ($140.0 \text{ m}^2 \cdot \text{g}^{-1}$). These results show the promising applications of Al_2O_3 as a catalyst support in the chemical industry.

Author Contributions: The manuscript was written by all the authors. D.L. and Y.F. conceived the project and oversaw all the research phases. Y.Z., Y.L. and Y.M. designed the project and collected and analyzed the data. Y.Z. and Y.L. built the activity testing equipment and performed the corresponding tests. Y.Z., Y.L., Y.M., H.L., P.T., D.L. and Y.F. discussed the results. Y.Z., H.L., P.T. and Y.F. wrote and revised the paper. All authors have read and agreed to the published version of the manuscript.

Funding: This research was funded by the National Key R&D Program of China, grant number 2016YFB0301600.

Data Availability Statement: Not applicable.

Conflicts of Interest: The authors declare no conflict of interest.

References

1. Xu, J.; Ibrahim, A.-R.; Hu, X.; Hong, Y.; Su, Y.; Wang, H.; Li, J. Preparation of large pore volume γ -alumina and its performance as catalyst support in phenol hydroxylation. *Microporous Mesoporous Mater.* **2016**, *231*, 1–8. [[CrossRef](#)]
2. Li, T.; Zhang, L.; Tao, Z.; Hu, C.; Zhao, C.; Yi, F.; Gao, X.; Wen, X.; Yang, Y.; Li, Y. Synthesis and characterization of amorphous silica-alumina with enhanced acidity and its application in hydro-isomerization/cracking. *Fuel* **2020**, *279*, 118487. [[CrossRef](#)]

3. Liu, P.; Feng, J.; Zhang, X.; Lin, Y.; Evans, D.G.; Li, D. Preparation of high purity spherical gamma-alumina using a reduction-magnetic separation process. *J. Phys. Chem. Solids* **2008**, *69*, 799–804. [[CrossRef](#)]
4. Delgado, A.D.; Alvarez-Contreras, L.; Beltran, K.A.; Leyva-Porras, C.; Aguilar-Elguezabal, A. Comparison of three-dimensional versus two-dimensional structure of mesoporous alumina as support of (Ni)MoS₂ catalysts for HDS. *Catal. Today* **2021**, *360*, 165–175. [[CrossRef](#)]
5. Rahmati, M.; Huang, B.; Mortensen, M.K., Jr.; Keyvanloo, K.; Fletcher, T.H.; Woodfield, B.F.; Hecker, W.C.; Argyle, M.D. Effect of different alumina supports on performance of cobalt Fischer-Tropsch catalysts. *J. Catal.* **2018**, *359*, 92–100. [[CrossRef](#)]
6. Shan, Y.-L.; Zhao, W.-T.; Zhao, S.-L.; Wang, X.-X.; Sun, H.-L.; Yu, W.-L.; Ding, J.-W.; Feng, X.; Chen, D. Effects of alumina phases on the structure and performance of VO_x/Al₂O₃ catalysts in non-oxidative propane dehydrogenation. *Mol. Catal.* **2021**, *504*, 111466. [[CrossRef](#)]
7. Lv, Y.; Li, D.; Tang, P.; Feng, Y. A simple and promoter free way to synthesize spherical γ -alumina with high hydrothermal stability. *Mater. Lett.* **2015**, *155*, 75–77. [[CrossRef](#)]
8. Nazer, S.; Dabbagh, H.A.; Najafi Chermahini, A.; Farrokhpour, H. Surface modification of alumina with P₂O₅ and its application in 2-octanol dehydration. *React. Kinet. Mech. Catal.* **2020**, *129*, 265–282. [[CrossRef](#)]
9. Enache, D.; Roy-Auberger, M.; Esterle, K.; Revel, R. Preparation of Al₂O₃-ZrO₂ mixed supports; their characteristics and hydrothermal stability. *Colloids Surf. A Physicochem. Eng. Asp.* **2003**, *220*, 223–233. [[CrossRef](#)]
10. Cheng, G.; Shen, G.; Wang, J.; Wang, Y.; Zhang, W.; Wang, J.; Shen, M. The Hydrothermal Stability and the Properties of Non- and Strongly-Interacting Rh Species over Rh/ γ , θ -Al₂O₃ Catalysts. *Catalysts* **2021**, *11*, 99. [[CrossRef](#)]
11. Zhang, Y.; Huang, B.; Mardkhe, M.K.; Woodfield, B.F. Thermal and hydrothermal stability of pure and silica-doped mesoporous aluminas. *Microporous Mesoporous Mater.* **2019**, *284*, 60–68. [[CrossRef](#)]
12. Claude, V.; Mahy, J.G.; Wolfs, C.; Lambert, S.D. Physico-chemical properties of alumina supports modified with silicon alkoxides. *J. Solid State Chem.* **2020**, *282*, 121102. [[CrossRef](#)]
13. Amrute, A.P.; Jeske, K.; Lodziana, Z.; Prieto, G.; Schueth, F. Hydrothermal Stability of High-Surface-Area alpha-Al₂O₃ and Its Use as a Support for Hydrothermally Stable Fischer-Tropsch Synthesis Catalysts. *Chem. Mater.* **2020**, *32*, 4369–4374. [[CrossRef](#)]
14. Chung, S.; Liu, Q.; Joshi, U.A.; Regalbuto, J.R.; Boateng, A.A.; Smith, M.A.; Coe, C.G. Using polyfurfuryl alcohol to improve the hydrothermal stability of mesoporous oxides for reactions in the aqueous phase. *J. Porous Mater.* **2018**, *25*, 407–414. [[CrossRef](#)]
15. Girel, E.; Cabiac, A.; Chaumonnot, A.; Besson, M.; Tuel, A. Selective Carbon Deposition on gamma-Alumina Acid Sites: Toward the Design of Catalyst Supports with Improved Hydrothermal Stability in Aqueous Media. *ACS Appl. Mater. Interfaces* **2020**, *12*, 13558–13567. [[CrossRef](#)]
16. Van Cleve, T.; Underhill, D.; Rodrigues, M.V.; Sievers, C.; Medlin, J.W. Enhanced Hydrothermal Stability of gamma-Al₂O₃ Catalyst Supports with Alkyl Phosphonate Coatings. *Langmuir* **2018**, *34*, 3619–3625. [[CrossRef](#)]
17. Pérez, L.L.; Alvarez-Galván, C.; Zarubina, V.; Fernandes, B.O.F.; Melián-Cabrera, I. A hydrothermally stable transition alumina by condensation-enhanced self-assembly and pyrolysis crystallization: Application in the steam reforming of methane. *CrystEngComm* **2014**, *16*, 6775–6783. [[CrossRef](#)]
18. Fujisaki, S.; Zahir, M.H.; Ikuhara, Y.H.; Iwamoto, Y.; Kuroda, K. Nanostructural Characterization of Hydrothermally Stable γ -Alumina-Based Composite Materials by Transmission Electron Microscopy. *Adv. Mater. Res.* **2007**, *26–28*, 1109–1112. [[CrossRef](#)]
19. Gu, Y.; Hacarlioglu, P.; Oyama, S.T. Hydrothermally stable silica-alumina composite membranes for hydrogen separation. *J. Membr. Sci.* **2008**, *310*, 28–37. [[CrossRef](#)]
20. Zhao, Y.; Li, F.; Zhang, R.; Evans, D.G.; Duan, X. Preparation of Layered Double-Hydroxide Nanomaterials with a Uniform Crystallite Size Using a New Method Involving Separate Nucleation and Aging Steps. *Chem. Mater.* **2002**, *14*, 4286–4291. [[CrossRef](#)]
21. Li, Z.J.; He, L.; Tian, W.L.; Huang, R.Y.; Wang, X.P.; Li, D.Q.; Tang, P.G.; Feng, Y.J. Batch and fixed-bed adsorption behavior of porous boehmite with high percentage of exposed (020) facets and surface area towards Congo red. *Inorg. Chem. Front.* **2021**, *8*, 735–745. [[CrossRef](#)]
22. Feng, Y.J.; Li, D.Q.; Li, C.X.; Wang, Z.H.; Evans, D.G.; Duan, X. Synthesis of Cu-containing layered double hydroxides with a narrow crystallite-size distribution. *Clays Clay Miner.* **2003**, *51*, 566–569. [[CrossRef](#)]
23. Yang, Y.; Xu, Y.; Han, B.; Xu, B.; Liu, X.; Yan, Z. Effects of synthetic conditions on the textural structure of pseudo-boehmite. *J. Colloid Interface Sci.* **2016**, *469*, 1–7. [[CrossRef](#)] [[PubMed](#)]
24. Coronado, I.; Stekrova, M.; Reinikainen, M.; Simell, P.; Lefferts, L.; Lehtonen, J. A review of catalytic aqueous-phase reforming of oxygenated hydrocarbons derived from biorefinery water fractions. *Int. J. Hydrogen Energy* **2016**, *41*, 11003–11032. [[CrossRef](#)]
25. Ravenelle, R.M.; Copeland, J.R.; Kim, W.G.; Crittenden, J.C.; Sievers, C. Structural Changes of gamma-Al₂O₃-Supported Catalysts in Hot Liquid Water. *ACS Catal.* **2011**, *1*, 552–561. [[CrossRef](#)]